ACS Macro Letters

Letter

pubs.acs.org/macroletters

One-Pot Synthesis of Hierarchically Macro- and Mesoporous Carbon Materials with Graded Porosity

Sarah A. Hesse,[†,‡,§] Jörg G. Werner,[†,‡,§] and Ulrich Wiesner*[,†]

[†]Department of Materials Science and Engineering and [‡]Department of Chemistry and Chemical Biology, Cornell University, Ithaca, New York 14850, United States

Supporting Information

ABSTRACT: Hierarchically porous materials are becoming increasingly important in catalysis, separation, and energy applications due to their advantageous diffusion and flux properties. Here we present the synthesis of hierarchically macro- and mesoporous carbon materials with graded porosity from a one-pot fabrication route. Organic−polymeric hybrids of a carbon precursor and poly(isoprene)-*block*-poly(styrene)-*block*-poly(4-vinylpyridine) with graded porosity are obtained via coassembly and nonsolvent-induced phase separation. The membranes were carbonized at temperatures as high as 1100 °C with simultaneous decomposition of the block copolymer. The carbon materials show an open nanoporous top surface with narrow pore-size distribution that opens up into a graded macroporous support with increasing macropore size along the film normal and mesoporous walls, providing for highly accessible porosity with a large surface area of over 500 m^2 g^{-1}. Further, we expand the direct synthesis process to form well-dispersed metal nanoparticles (such as nickel and platinum) on the graded, hierarchically porous carbon materials. Our one-pot synthesis offers a facile approach to graded macro- and mesoporous carbons.

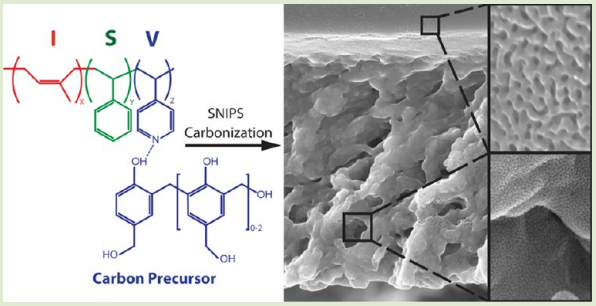

Mesoporous materials have been used for a wide range of applications including biomedical implants, water filtration, and energy devices, due to their high surface areas and pore volumes. In particular, mesoporous inorganic materials such as carbon, metal, and metal oxide materials have been employed for energy conversion and storage applications, as well as catalysis and separation.[1−9]

In order to increase the accessibility of mesoporous materials and to promote diffusion and material flux for both gases and liquids, hierarchical meso- and macroporosity has been demonstrated to be advantageous. Furthermore, graded macroporosity featuring a continuous increase in pore size along at least one direction can combine high material flux with good separation resolution in membrane applications.[10,11] Graded porosity has also shown promise in minimizing mass transport resistance to either liquids or gases as well as increasing catalyst utilization and power density in fuel cell electrode materials.[12,13]

Combining the synthesis of inorganic materials with polymer fabrication techniques in soft- or hard-templating processes opens the door to facile scalability and compatibility with role-to-role processing for low-cost, large-area fabrication. Numerous ordered mesoporous carbons from block copolymer (BCP) soft-templating have been reported with pore sizes of below 15 nm for Pluronics templates and up to 40 nm with high molar mass BCPs. Surface areas range from 150 to 1000 m^2 g^{-1}, dependent on pore size, carbonization temperature, and microporosity.[14−19] Only a few hierarchical macro- and mesoporous carbons have been reported using one-pot hydrothermal synthesis or spinodal decomposition.[20,21] Recently, BCPs have been used for the fabrication of graded, hierarchically macro- and mesoporous polymer membranes with ordered features on the nanoscale via the self-assembly and nonsolvent-induced phase separation (SNIPS) process.[10,11,22−24] These SNIPS-casted polymeric membranes have been utilized as sacrificial polymeric hard templates for the synthesis of carbon, metal, and metal oxide materials with graded macro- and mesoporosity (Cornell Graded Materials: CGM); however, hard-templating approaches are often lengthy and tedious.[25] Here, we demonstrate the first direct one-pot synthesis of graded macro- and mesoporous carbon material (CGM-C).

The CGM-Cs exhibit an open nanoporous surface with narrow pore size distribution on top of a macroporous substructure with graded macroporosity toward the bottom. The macroporous carbon substructure consists of mesoporous walls. This hierarchical porosity leads to easily accessible high surface area of over 500 m^2 g^{-1}, which is within the typically observed range for mesoporous carbons.[16] Furthermore, we expand the process to form well-dispersed metal nanoparticles (NPs) such as nickel and platinum on the CGM-C.

CGM-Cs were obtained using coassembly and nonsolvent-induced phase separation of poly(isoprene)-*block*-poly-

Received: February 6, 2015
Accepted: April 8, 2015
Published: April 13, 2015

DOI: 10.1021/acsmacrolett.5b00095
ACS Macro Lett. 2015, 4, 477−482

Scheme 1. CGM-C Fabrication Process: A Solution Consisting of ISV and Resols in a 7:3 wt % DOX:THF Mixture Is Cast onto a Glass Slide, Evaporated for a Specific Amount of Time to Induce a Concentration Gradient, and Plunged into a DI Water Bath, Which Converts the Concentration into a Structural Gradient[a]

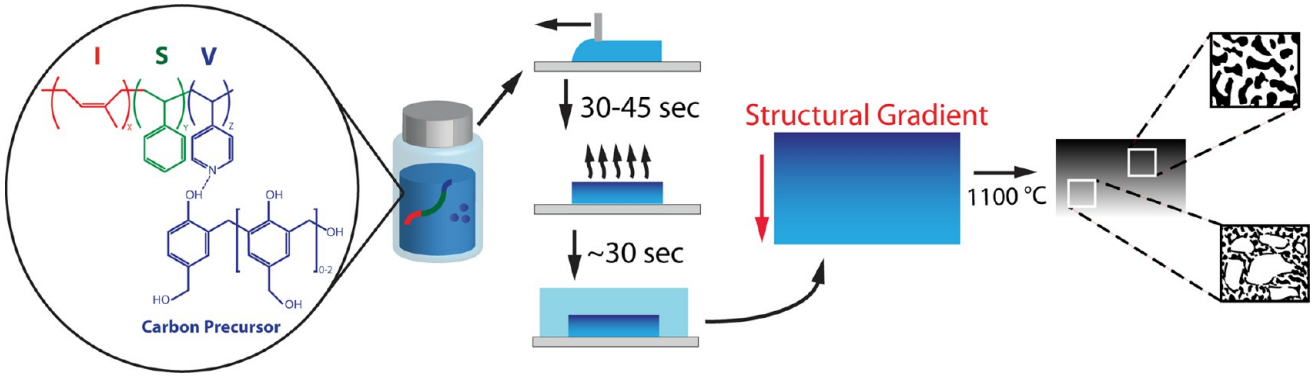

[a]Resols are cross-linked at 90 °C and subsequently carbonized at 1100 °C. The BCP decomposes during carbonization leading to shrinkage of the structure and mesoporosity (right inset).

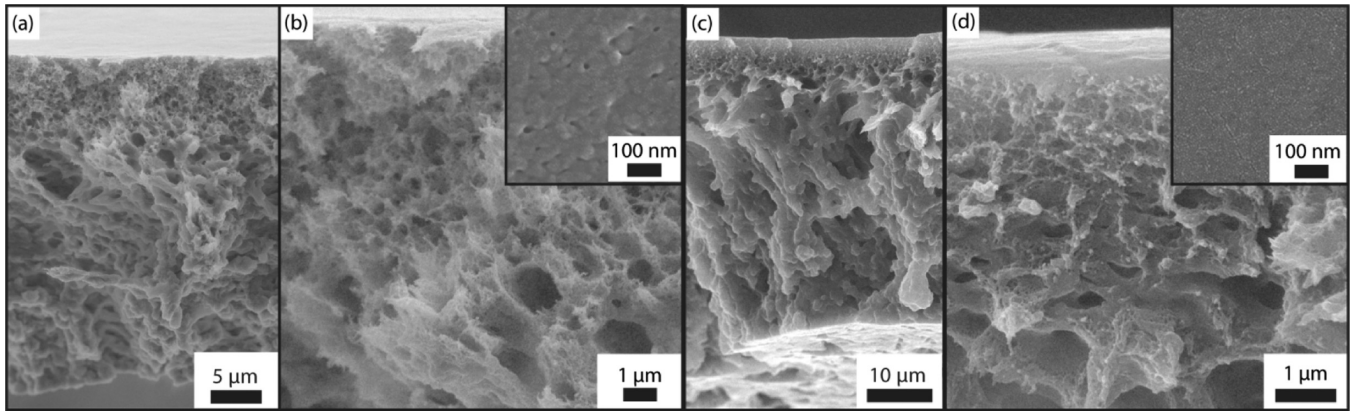

Figure 1. SEM images of an organic−polymeric hybrid membrane cast from a 12 wt % polymer and resols (2:1 wt ratio) solution and evaporated for 33 s. (a) 30 μm sponge-like cross-section of the as-cast membrane. (b) Cross-section of the upper part at higher magnification. The top surface is shown in the inset of (b), indicating mesoporosity through the top layer. (c) Cross-sectional image of the same membrane post-90 °C cross-linking. (d) Top part of the cross-section at higher magnification. The top surface is shown in the inset, indicating a closed surface after curing of the hybrid membrane.

(styrene)-*block*-poly(4-vinylpyridine) (ISV) and phenol-formaldehyde resols. The ISV terpolymer employed here had a molar mass of 103 kg/mol, a polydispersity index (PDI) of 1.11, and weight fractions of 25%, 57%, and 18% for poly(isoprene) (PI), poly(styrene) (PS), and poly(4-vinylpyridine) (P4VP), respectively.[10] Phenol-formaldehyde resols with a molar mass of less than 500 g/mol were used as thermally cross-linkable carbon precursors.[19]

ISV terpolymer and carbon precursors were dissolved (2:1 by weight) in a 1,4-dioxane (DOX) to tetrahydrofuran (THF) mixture (7:3 by weight) as an overall 12 wt % solution (8 wt % with respect to the ISV polymer). Terpolymer composition and casting conditions were based on our experience with SNIPS-derived ISV membranes and optimized for this system.[10,22−24] The carbon precursors increase the viscosity of the casting solution, allowing a lower polymer concentration as compared to pure ISV-membrane formation using SNIPS.[10] Hydrophilic carbon precursors attach to the P4VP block via hydrogen bonding to the nitrogen of the pyridine ring.[26,27] The homogeneous solution was cast on glass slides using a doctor blade. After partial evaporation of the solvents for a specific time (i.e., 33 s) inducing a concentration gradient along the film-normal direction, films were plunged into a water bath for nonsolvent-induced phase separation (NIPS, Scheme 1). Precipitation of the glassy PS block induced increasing macroporosity along the concentration gradient from the top to the bottom of the membranes. Short time periods of membranes in the nonsolvent water bath (<30 s) avoided excessive dissolution of the water-soluble phenol-formaldehyde resols. Longer time periods caused the resols to dissipate from the membranes, thereby significantly decreasing the carbon yield during the carbonization process. As such, immersing membranes in a water bath overnight yielded membrane structures similar to the ones described here but did not allow for carbonization (Figure S1, Supporting Information). The ISV−resols hybrid membranes were subsequently dried and further cured at 90 °C. The curing step (cross-linking of the resols) is essential to provide a stable structure upon carbonization. Figure 1a shows the 30 μm thick cross-section of a dried ISV−resols membrane with graded macroporosity. A few microns thick mesoporous layer (enlarged in Figure 1b) sits on top of a macroporous support layer with increasing macropore size from top to bottom. For comparison, Figure S2 (Supporting Information) provides a cross-sectional and top surface SEM image of a pure ISV membrane (i.e., without resols) cast from a 12 wt % ISV solution and evaporated for

DOI: 10.1021/acsmacrolett.5b00095
ACS Macro Lett. 2015, 4, 477−482

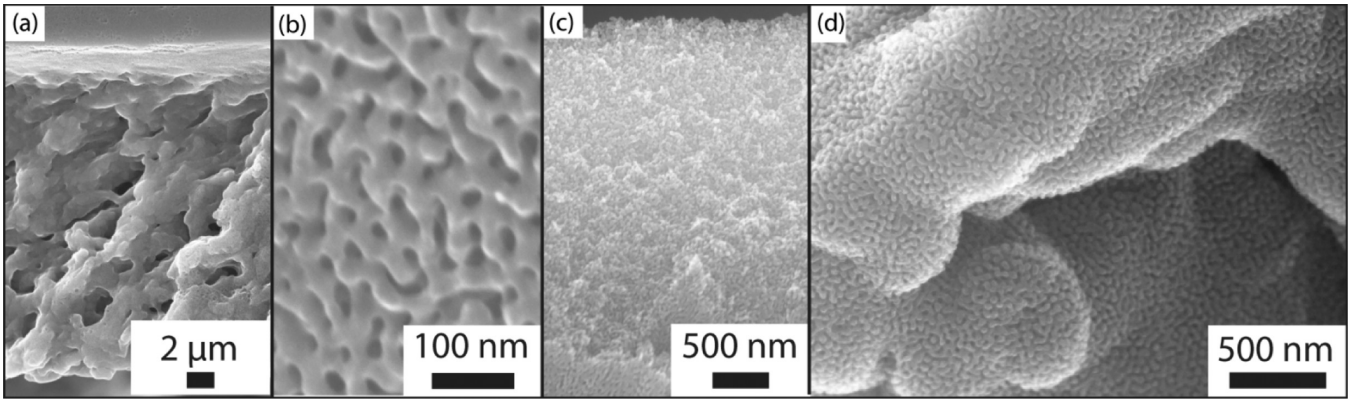

Figure 2. SEM images of a graded, hierarchically porous carbon material (CGM-C) after heat treatment at 1100 °C. (a) Full cross-section demonstrating the graded macroporosity. (b) Top surface with homogeneous mesoporosity. (c) Cross-section of the mesoporous top part of the carbon membrane at higher magnification. (d) Cross-section of the macroporous bottom part of the carbon membrane showing the hierarchical macro-/mesoporosity.

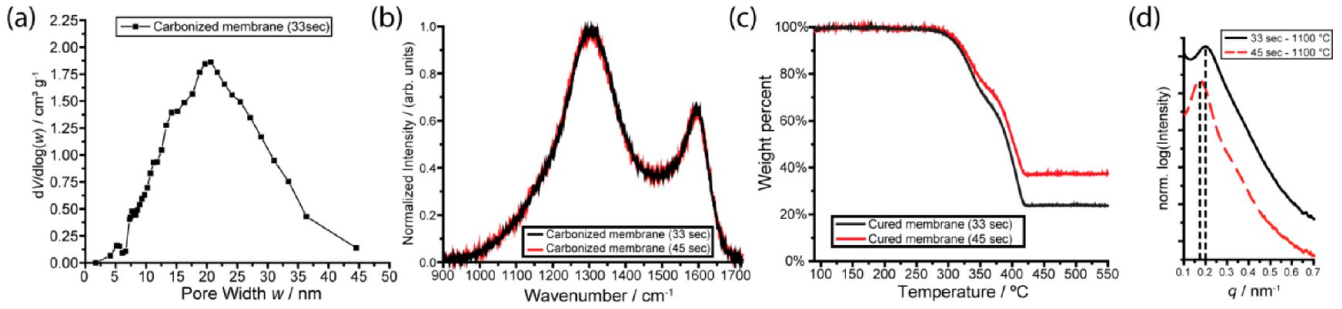

Figure 3. (a) BJH pore size distribution of the carbonized material (1100 °C) cast from a 12 wt % polymer and resols (2:1 wt ratio) solution and evaporated for 33 s. (b–d) Characterization results of materials obtained under identical processing conditions but from 33 s (black) and 45 s (red) evaporation times, respectively. (b) Raman spectra for carbonized samples (1100 °C) with D- and G-bands. (c) TGA curves of these membranes. (d) SAXS curves of carbonized materials (1100 °C).

45 s. The organic–polymeric hybrid and neat ISV terpolymer membranes exhibit similar cross-sectional structures. The top surface of the as-cast hybrid, however, shows only some degree of mesoporosity without order (inset in Figure 1b), very different from the square packing of mesopores in the neat ISV terpolymer membrane. After curing of the resols at 90 °C the structure remains asymmetric and porous (Figure 1c,d). However, the walls of the cured hybrid appear to be smoother, and the top surface of the film exhibits no porosity (Figure 1d). We speculate that this is due to the mobility of the resols and polymer at the elevated temperature that causes a decrease in surface roughness during curing.

The cured organic–polymeric hybrid membranes were carbonized at 1100 °C under an inert atmosphere (nitrogen flow). The phenol-formaldehyde resols further condense and carbonize at higher temperatures (>600 °C), while the triblock terpolymer decomposes, thereby forming graded carbon materials with hierarchical porosity (CGM-C, Figure 2). The overall structure is well maintained despite significant shrinkage of the membranes during carbonization that is due to the considerable amount of ISV terpolymer that decomposes between 300 and 400 °C (Figure 3c). Carbonized materials are more fragile than the as-cast and post-90 °C membranes but maintain their monolithic shape. The cross-section in Figure 2a of a carbonized membrane shows graded macroporosity with a 2–3 μm thick mesoporous layer (enlarged in Figure 2c) on top of a 20 μm macroporous substructure. The top surface of the carbonized membrane shows network-like mesoporosity with homogeneous pore sizes of about 12–14 nm (Figure 2b). An important feature of this carbonized material is that the walls of the macropores are in turn mesoporous (Figure 2d), constituting the structural hierarchy with simultaneous macropore gradation from top to bottom. Analysis of the nitrogen adsorption isotherm (Figure S4, Supporting Information) according to the Brunauer–Emmett–Teller (BET) theory yielded a surface area of 547 $m^2\ g^{-1}$.[28] The nitrogen sorption isotherms show a typical type-IV curve with H_1-type hysteresis and sharp capillary condensations above relative pressures of 0.9, with a total mesopore volume of 1.0 $cm^3\ g^{-1}$ calculated at a relative pressure of 0.99. The BJH pore size distribution (Figure 3a) peaks at 20 nm with a full-width at half-maximum (fwhm) of 19 nm.[29]

Raman spectra from the graded, hierarchically porous membranes carbonized at 1100 °C corroborate the formation of disordered carbon materials (Figure 3b). The typical D-band and G-band appear at 1306 and 1590 cm^{-1}, respectively.[30,31] To illustrate the effects of the nonsolvent-induced phase separation and the microphase separation of the ISV triblock terpolymer, we also casted a film that was completely dried (evaporation at room temperature for over 2.5 min) before immersion in the water bath. Figure S3 (Supporting Information) provides SEM images of the fully dried film after carbonization, cast from the same ISV–resols solution described above. The 15 μm thick carbon film exhibited a disordered, mesoporous network structure without macroporosity. The dried and cured films did not show any porosity

DOI: 10.1021/acsmacrolett.5b00095
ACS Macro Lett. 2015, 4, 477–482

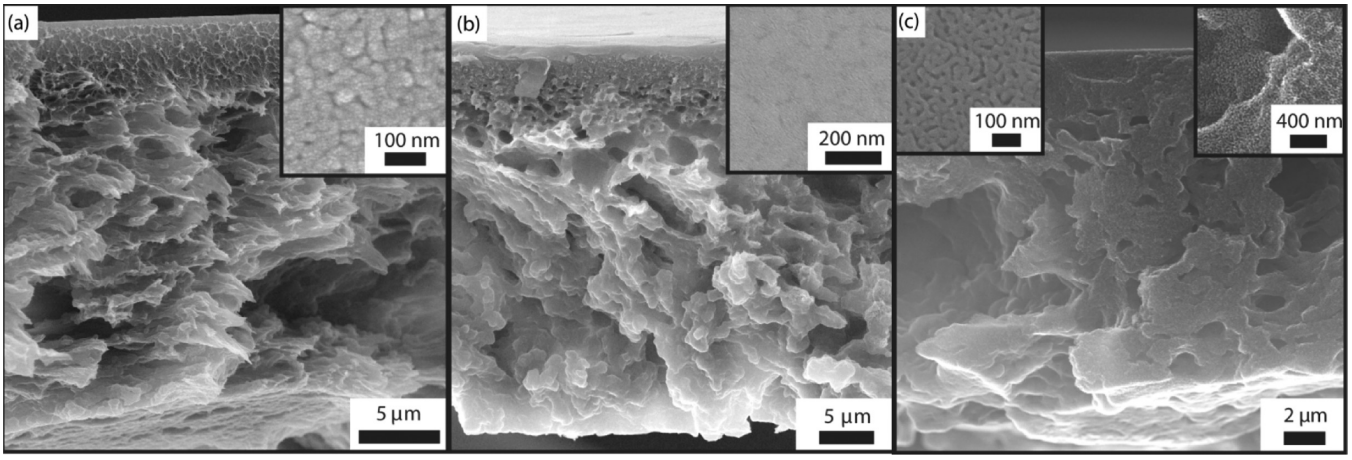

Figure 4. SEM images of the membrane cast from 12 wt % polymer and resol (2:1 wt ratio) solution evaporated for 45 s at different processing stages. (a) 23 μm thick sponge-like cross-section of the as-cast membrane. Inset shows the top surface with mesostructural features and low porosity. (b) Cross-section of the same membrane post-90 °C cross-linking. Inset shows the smooth top surface without significant structural features. (c) Cross-section of the carbonized (1100 °C) material. Insets show top surface with homogeneous mesoporous features (left) and macroporous bottom part (right) demonstrating hierarchical macro-/mesoporosity.

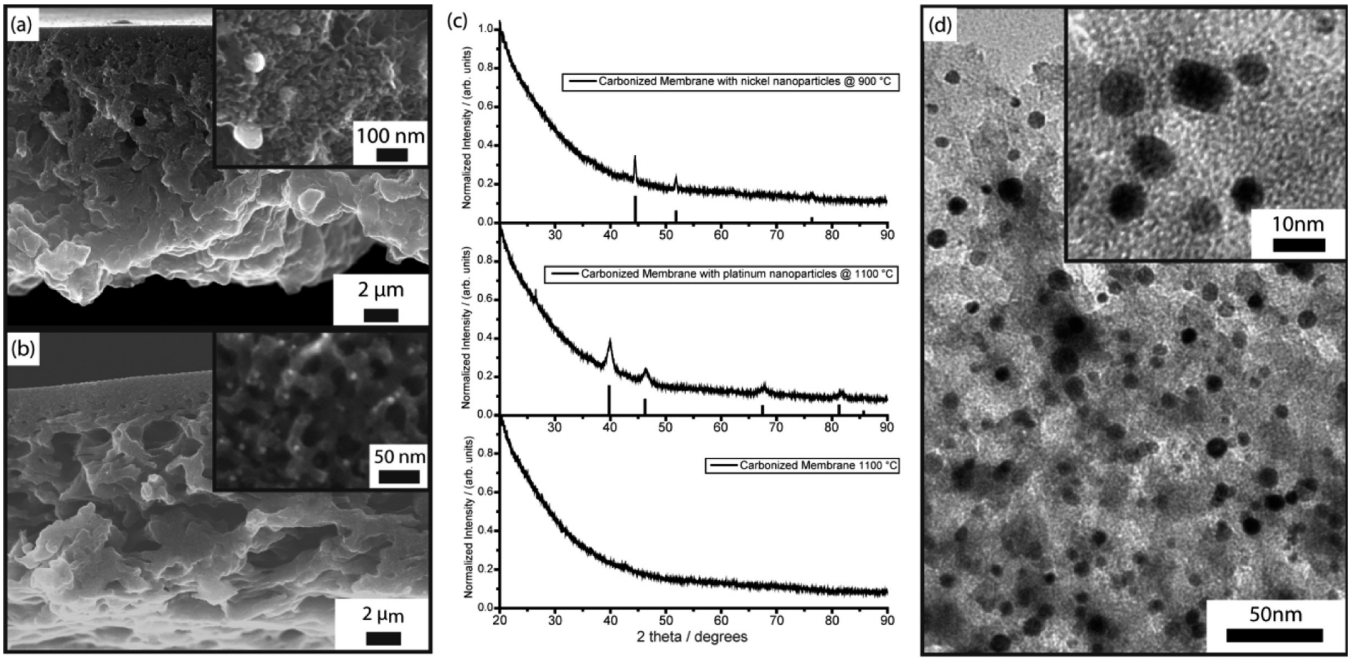

Figure 5. (a,b) SEM images of graded, hierarchically porous carbon membranes containing Ni (a) and Pt (b) NPs (900 and 1100 °C carbonization temperatures, respectively). Insets show mesoporous parts at higher magnification with dispersed large Ni and small Pt NPs. (c) XRD data of the carbonized membranes with Ni (top) and Pt (middle) NPs. For comparison, the XRD pattern of the carbonized membrane without metal NPs is shown on the bottom. (d) TEM image of a mesoporous part of the carbonized membrane exhibiting well-dispersed Pt NPs in the mesopores.

(data not shown). This suggests that the formation of the graded hierarchical porosity is due to the NIPS process, while ISV decomposition of the microphase-separated ISV−resols composite most likely contributes to the mesoporosity of the final membranes.

In order to investigate the effect of evaporation time on membrane structure, another membrane was cast from the same solution as above but with a 45 s evaporation time before plunging into the nonsolvent bath. Figure 3b provides thermogravimetric analysis (TGA) data of the cured membranes with evaporation times of 33 and 45 s in black and red, respectively. Both curves show the same qualitative shape, with the onset temperature for terpolymer decomposition at 300 °C and full decomposition at 420 °C. The phenol-formaldehyde resin left at the final temperature comprised 20 and 35 wt % of the original hybrid in the case of 33 and 45 s evaporation time, respectively. We speculate that the higher ISV−resols concentration after longer evaporation time results in better retention of the resols during the nonsolvent plunge, thereby allowing for a higher yield during carbonization. No difference in graphitization was observable from Raman spectroscopy between the two CGM-Cs obtained from different evaporation times (Figure 3b).

Small-angle X-ray scattering (SAXS) traces of the carbonized membranes (1100 °C) reveal correlation lengths of the disordered mesostructure of 32 and 36 nm for evaporation

DOI: 10.1021/acsmacrolett.5b00095
ACS Macro Lett. 2015, 4, 477−482

times of 33 and 45 s, respectively (Figure 3c). This result is consistent with the TGA data, as longer evaporation times allow more resols to be incorporated in the membrane, which causes less shrinkage during pyrolysis. Membranes before carbonization did not show any peaks in SAXS (data not shown), most likely due to the low electron density contrast between the phases in the ISV−resols hybrids.

Figure 4 depicts SEM images of a membrane that was cast with an evaporation time of 45 s. While the membrane appears denser (e.g., see 23 μm thick cross-section in Figure 4a), the overall features of the membrane are similar to those after only 33 s evaporation time shown in Figure 1. This is expected as the increased evaporation time causes a decrease of solvent content at the time of NIPS. The top surface and cross-sectional structural features evolve in a similar way during curing at 90 °C (Figure 4b) and carbonization at 1100 °C (Figure 4c) as described above for the membrane with shorter evaporation time. Longer evaporation time leads to a smaller top surface mesopore size of only about 8−10 nm, however (left inset of Figure 4c).

In order to further show the versatility of our approach and to increase functionality, we incorporated metal NPs into CGM-Cs. To that end, in addition to the terpolymer and carbon precursor, membranes were cast from solutions containing (1,5-cyclooctadiene) dimethyl platinum(II) or bis(cyclopentadienyl) nickel(II) (1:4 or 1:10 ratio to resols by weight, respectively) for the synthesis of well-dispersed platinum or nickel NPs, respectively (Pt/Ni-NPs-on-CGM-C). The metal precursors were reduced during the heat treatment under inert gas and formed well-dispersed metal NPs on the carbon walls throughout the entire hierarchically porous carbon membrane. Figure 5 shows SEM images of the graded NP-on-CGM-Cs after pyrolysis, together with the corresponding X-ray diffraction (XRD) patterns. A marked Figure 5 indicating the exact positions of nickel and platinum nanoparticles can be found in the Supporting Information (Figure S5). The cross-section of Ni-NP-on-CGM-C after carbonization at 900 °C shows graded macroporosity, very similar to the neat carbon membranes. Large nickel NPs with diameters of 50−70 nm are well dispersed in the mesoporous parts of the carbon material (Figure 5a, inset). The corresponding XRD pattern shows the expected peaks for fcc nickel (top of Figure 5c, PDF-card 01-073-6826). The average domain size of 40 nm was approximated using the Scherrer equation on the (111), (200), and (220) peaks. The cross-section of Pt-NPs-on-CGM-C is shown in Figure 5b. Small NPs are well dispersed on the mesoporous walls (Figure 5b, inset) throughout the membrane without disrupting the membrane morphology. The broad peaks in the corresponding XRD pattern (middle panel in Figure 5c) corroborate formation of small platinum crystallites (PDF-card 01-087-0646) with an average domain size of 3 nm, approximated using the Scherrer equation for the first four peaks. The transmission electron microscopy (TEM) micrograph in Figure 5d shows small platinum NPs with diameters ranging from 6 to 10 nm well dispersed in the mesoporous parts of the carbonized membrane. The different mean dimensions, as evident from XRD and TEM analysis, indicate the presence of multidomain NPs. The incorporation of metal NPs was achieved with almost no alteration to the protocol despite the inclusion of a soluble metal precursor to the initial casting solution, demonstrating the versatility of the synthesis protocol.

In conclusion, we reported on a facile one-pot synthesis method to create hierarchically macro- and mesoporous carbon materials with graded porosity (CGM-C). These membranes with a typical thickness of tens of microns possess a nanoporous top surface with narrow pore size distribution on top of a graded macroporous support structure that in turn exhibits mesoporous walls. This allows for highly accessible porosity with large surface areas. Furthermore, we demonstrated that the direct synthesis can conveniently be expanded to include metal precursors for the fabrication of graded, hierarchically porous carbon structures with well-dispersed metal NPs. Due to the advantageous structural and porosity features we expect that these carbon structures will find use in a variety of applications including energy conversion and storage, catalysis, and separation.

■ ASSOCIATED CONTENT

Supporting Information

Experimental procedures, SEM images of ISV membranes and mesoporous cabons, nitrogen sorption isotherms, and Figure 5 with labeled nickel and platinum NPs. This material is available free of charge via the Internet at http://pubs.acs.org.

■ AUTHOR INFORMATION

Corresponding Author

*E-mail: ubw1@cornell.edu.

Author Contributions

§(S.A.H., J.G.W.) These authors contributed equally to this work.

Notes

The authors declare no competing financial interest.

■ ACKNOWLEDGMENTS

This project was funded by the National Science Foundation (DMR-1409105). The work made further use of the Cornell Center for Materials Research Shared Facilities, which are supported through the NSF MRSEC program (DMR-1120296). The authors thank Prof. Sol Gruner (Cornell University) for his kind assistance with SAXS measurements.

■ REFERENCES

(1) Rolison, D. R.; Long, J. W.; Lytle, J. C.; Fischer, A. E.; Rhodes, C. P.; McEvoy, T. M.; Bourg, M. E.; Lubers, A. M. *Chem. Soc. Rev.* **2009**, *38*, 226−252.
(2) Tappan, B. C.; Steiner, S. A.; Luther, E. P. *Angew. Chem., Int. Ed. Engl.* **2010**, *49*, 4544−4565.
(3) Orilall, M. C.; Wiesner, U. *Chem. Soc. Rev.* **2011**, *40*, 520−535.
(4) Lakes, R. *Nature* **1993**, *361*, 511−515.
(5) Kresge, C. T.; Leonowicz, M. E.; Roth, W. J.; Vartuli, J. C.; Beck, J. S. *Nature* **1992**, *359*, 710−712.
(6) Yang, P. D.; Zhao, D. Y.; Margolese, D. I.; Chmelka, B. F.; Stucky, G. D. *Nature* **1998**, *396*, 152−155.
(7) Joo, S. H.; Choi, S. J.; Oh, I.; Kwak, J.; Liu, Z.; Terasaki, O.; Ryoo, R. *Nature* **2001**, *412*, 169−172.
(8) Warren, S. C.; Messina, L. C.; Slaughter, L. S.; Kamperman, M.; Zhou, Q.; Gruner, S. M.; DiSalvo, F. J.; Wiesner, U. *Science* **2008**, *320*, 1748−1752.
(9) Wang, D. W.; Li, F.; Liu, M.; Lu, G. Q.; Cheng, H. M. *Angew. Chem., Int. Ed.* **2008**, *47*, 373−376.
(10) Phillip, W. a; Dorin, R. M.; Werner, J.; Hoek, E. M. V; Wiesner, U.; Elimelech, M. *Nano Lett.* **2011**, *11*, 2892−2900.
(11) Peinemann, K.; Abetz, V.; Simon, P. F. W. *Nat. Mater.* **2007**, *6*, 992−996.
(12) Litster, S.; McLean, G. *J. Power Sources* **2004**, *130*, 61−76.

DOI: 10.1021/acsmacrolett.5b00095
ACS Macro Lett. 2015, 4, 477−482

(13) Hamedani, H. A.; Baniassadi, M.; Khaleel, M.; Sun, X.; Ahzi, S.; Garmestani, H. *J. Power Sources* **2011**, *196*, 6325−6331.
(14) Liang, C.; Hong, K.; Guiochon, G. A.; Mays, J. W.; Dai, S. *Angew. Chem., Int. Ed. Engl.* **2004**, *43*, 5785−5789.
(15) Tanaka, S.; Nishiyama, N.; Egashira, Y.; Ueyama, K. *Chem. Commun. (Cambridge, U. K.)* **2005**, 2125−2127.
(16) Meng, Y.; Gu, D.; Zhang, F.; Shi, Y.; Yang, H.; Li, Z.; Yu, C.; Tu, B.; Zhao, D. *Angew. Chem., Int. Ed.* **2005**, *44*, 7053−7059.
(17) Kosonen, H.; Valkama, S.; Nykänen, A.; Toivanen, M.; ten Brinke, G.; Ruokolainen, J.; Ikkala, O. *Adv. Mater.* **2006**, *18*, 201−205.
(18) Deng, Y.; Yu, T.; Wan, Y.; Shi, Y.; Meng, Y.; Gu, D.; Zhang, L.; Huang, Y.; Liu, C.; Wu, X.; Zhao, D. *J. Am. Chem. Soc.* **2007**, *129*, 1690−1697.
(19) Werner, J. G.; Hoheisel, T. N.; Wiesner, U. *ACS Nano* **2014**, *8*, 731−743.
(20) Huang, Y.; Cai, H.; Feng, D.; Gu, D.; Deng, Y.; Tu, B.; Wang, H.; Webley, P. a; Zhao, D. *Chem. Commun. (Cambridge, U. K.)* **2008**, 2641−2643.
(21) Liang, C.; Dai, S. *Chem. Mater.* **2009**, *21*, 2115−2124.
(22) Gu, Y.; Dorin, R. M.; Wiesner, U. *Nano Lett.* **2013**, *13*, 5323−5328.
(23) Dorin, R. M.; Phillip, W. a.; Sai, H.; Werner, J.; Elimelech, M.; Wiesner, U. *Polymer (Guildf)* **2014**, *55*, 347−353.
(24) Dorin, R. M.; Marques, D. S.; Sai, H.; Vainio, U.; Phillip, W. A.; Peinemann, K.; Nunes, S. P.; Wiesner, U. *ACS Macro Lett.* **2012**, *1*, 614−617.
(25) Gu, Y.; Werner, J. G.; Dorin, R. M.; Robbins, S. W.; Wiesner, U. *Nanoscale* **2015**, *7*, 5826−5834.
(26) Florent, M.; Xue, C.; Zhao, D.; Goldfarb, D. *Chem. Mater.* **2012**, *24*, 383−392.
(27) Ruokolainen, J.; Saariaho, M.; Ikkala, O.; Ten Brinke, G.; Thomas, E. L.; Torkkeli, M.; Serimaa, R. *Macromolecules* **1999**, *32*, 1152−1158.
(28) Brunauer, S.; Emmett, P. H.; Teller, E. *J. Am. Chem. Soc.* **1938**, *60*, 309−319.
(29) Barrett, E. P.; Joyner, L. G.; Halenda, P. P. *J. Am. Chem. Soc.* **1951**, *73*, 373−380.
(30) Ferrari, a.; Robertson, J. *Phys. Rev. B* **2000**, *61*, 14095−14107.
(31) Tuinstra, F.; Koenig, L. *J. Chem. Phys.* **1970**, *53*, 1126−1130.

DOI: 10.1021/acsmacrolett.5b00095
ACS Macro Lett. 2015, 4, 477−482